Secondary Reconnection in Turbulent Reconnection Outflows

Giovanni Lapenta[1]†, Andrey Divin[2], Martin Goldman[3], David L. Newman[3], Vyacheslav Olshevsky[1] and Francesco Pucci[1]

[1]Depatment of Mathematics, KULeuven University, Leuven, Belgium
[2]Department of Physics, University of St Petersbourg, St Petersbourg, Russia
[3]University of Colorado, Boulder, USA

(Received xx; revised xx; accepted xx)

Reconnection outflows are regions of intense recent scrutiny, from in situ observations and from simulations. These regions are host to a variety of instabilities and intense energy exchanges, often even superior to the main reconnection site. We report here a number of results drawn from investigation of simulations. First, the outflows are observed to become unstable to drift instabilities . Second, these instabilities lead to the formation of secondary reconnection sites. Third, the secondary processes are responsible for large energy exchanges and particle energization. Finally, the particle distribution function are modified to become non-maxwellian and include multiple interpenetrating populations.

1. Introduction

Kinetic reconnection is fast, developing on Alfvén times, but also very localized. In many astrophysical and laboratory systems, large amounts of energy are converted over large domains. How can we bring fast kinetic reconnection to large scales? A possible scenario to reach large energy conversion rates on system scales is to imagine a situation where the initiation of reconnection is followed by a chain reaction of more and more secondary reconnection sites.

Three dimensional reconnection is accompanied by many more instabilities than two dimensional reconnection. Lapenta *et al.* (2015) focused on the development in reconnection outflows of instabilities that lead to secondary reconnection. Outflows from reconnection are rich in free energy that can drive instabilities. Among the possibilities we consider here:

- Velocity shears around the outflow jet that can drive Kelvin-Helmholtz instability.
- Density and temperature gradients at the front formed by the outflowing jet interacting with the ambient plasma leads to drift-type instabilities.
- Unfavourable curvature of field lines between the separatrices in the outflow region can lead to interchange (Rayleigh-Taylor-type) instabilities.
- Flux ropes in the outflows may be kink instability.
- Additional instabilities are caused by phase-space features such as anisotropies leading to whistler waves and beams leading to streaming instabilities.

All these instabilities can cause strong deformation of the flow, leading possibly to turbulence, energy exchange and secondary reconnection.

† Email address for correspondence: giovanni.lapenta@kuleuven.be

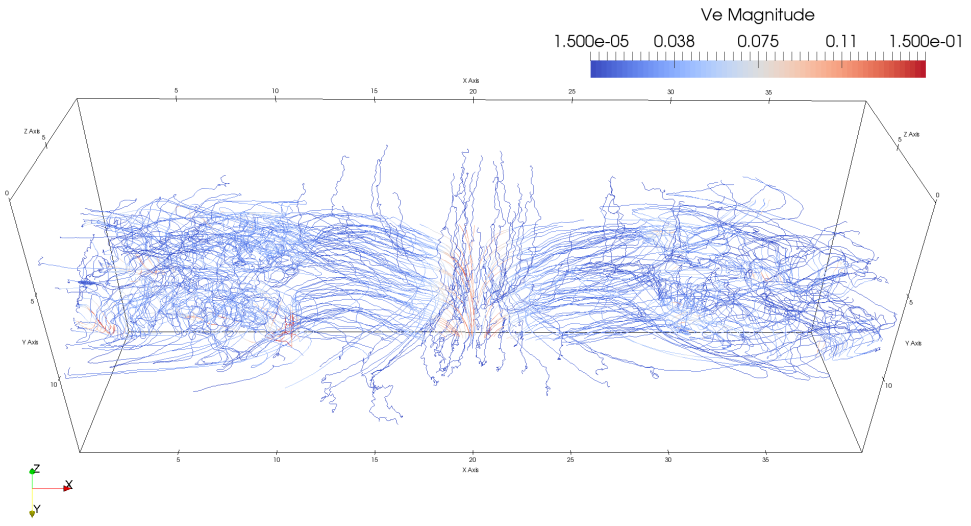

FIGURE 1. Visualization of the electron flow around a reconnection site. We report streamlines of the first order moment of the electron distribution (the electron flow velocity) coloured by the intensity of the local electron speed (normalized to the speed of light).

2. Development of outflow instabilities and secondary reconnection

We consider here the same run previously considered in Lapenta *et al.* (2015). The system is initialized with a Harris equilibriumHarris (1962) uniquely specified by the mass ratio $m_i/m_e = 256$, the temperature ratio $T_i/T_e = 5$ and $v_{th,e}/c = 0.045$. We add a uniform plasma background of 1/10 of the peak Harris density and a guide field of 1/10 of the lobe Harris field. The evolution is followed using the fully electromagnetic and fully kinetic iPic3D codeMarkidis *et al.* (2010) that treats both electrons and ions as particles. Details are provided in Lapenta *et al.* (2015). We use coordinates where x is along the initial magnetic field, y is along the initial gradients, and z is along the initial current.

Reconnection is initialised in the centre with an initial x-shaped perturbation that leads to the formation of a central x-line. A reconnection site develops with plasma accelerated towards the reconnection region and expelled out of it. The electron flow pattern in the fully developed non-linear stage is shown in Fig. 1. The electrons are first attracted toward the central x-line where the z-directed reconnection electric field accelerates them to high speed. The Lorentz force then deflects the particles towards the outflow. In this region, the system presents a remarkable invariance along z, resembling the same physics of two dimensional fast kinetic reconnection.

In the outflow, however, the electron flow pattern becomes distorted and meanders about, eventually passing downstream away of the reconnection region. In this region the electron flow becomes more turbulent.

The region of electron meandering corresponds to the front formed by the interaction of the outflowing plasma with the surrounding media. At the front, an effect similar to that of a snowplow pushes the plasma outward. A form forms where at least three of the mechanisms mentioned above are present: the field lines wrap around the front gaining unfavourbale curvature that can lead to interchange-type instabilities, the density

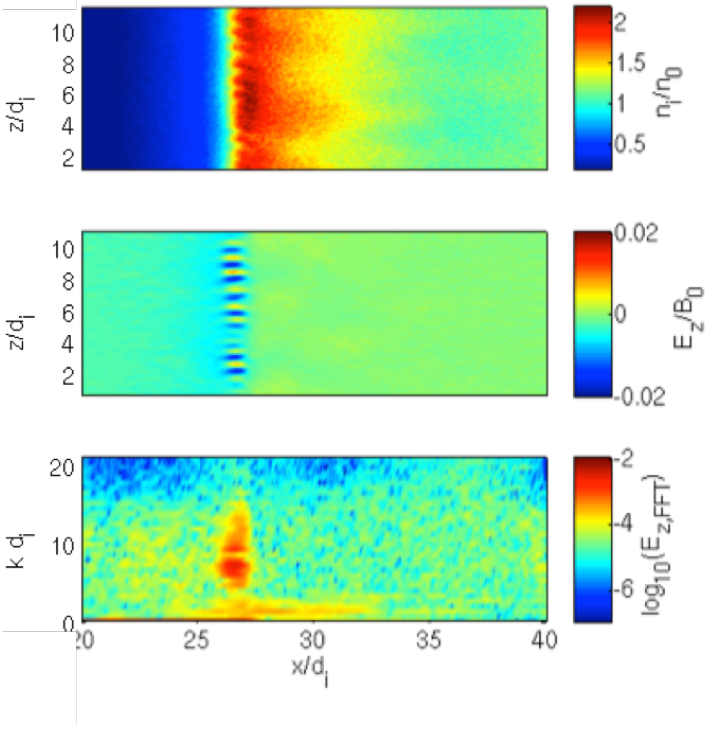

FIGURE 2. Early stages of the instability at the front, at time $\omega_{ci} = 15$. The panels show from top to bottom: ion density (a), z-component of the electric field (b) and the Fourier spectrum in k_zo f the perturbation of the electric field E_z.

gradient is unstable to drift modes and the distribution function becomes severely non-maxwellian leading to microinstabilities.

Figure2 shows the state of the front after the instability starts to develop. The density (panel a) becomes rippled by a mode that presents a strong perturbation of the E_z (panel b). When the mode structure of these fluctuations is Fourier analysed, the resulting spectrum in k_z is reported in panel c. The observed features are characteristic of a drift mode in the lower-hybrid range.

The identification of the instability as having primarily the nature of a lower-hybrid drift instability (LHDI) is confirmed by the temporal spectrum measured at a fixed point reached by the front (Divin *et al.* 2015*b*,*a*). A spectrogram, obtained with standard windowing methods similar to those used on-board real space probes, is reported: the observed frequency spectrum is reported at different times. The lower panel reports the corresponding observed local magnetic field intensity. When the front arrives, an intense signal in the lower hybrid range is measured.

As the evolution is continued, the ripples in the front become more intense and start to interact leading to conditions where magnetic field of opposite polarity is brought in contact promoting secondary reconnection. Figure 4 shows the front at two consecutive times: at later times, the "fingers" formed in the front tend to interact and coalesce Vapirev *et al.* (2013).

Lapenta *et al.* (2015) analysed several indicators to detect positively secondary reconnection sites: direct analysis of field line connectivity, energy dissipation in the electron frame ($\mathbf{J} \cdot (\mathbf{E} + \mathbf{v}_e \times \mathbf{B})$) electron agyrotropy, slippage ($\mathbf{v}_{e\perp} - \mathbf{E} \times \mathbf{B}/B^2$), topological measure of field line breakage (Hesse & Schindler 1988; Biskamp 2000) ($\mathbf{b} \times \nabla \times (E_{||}\mathbf{b})$,

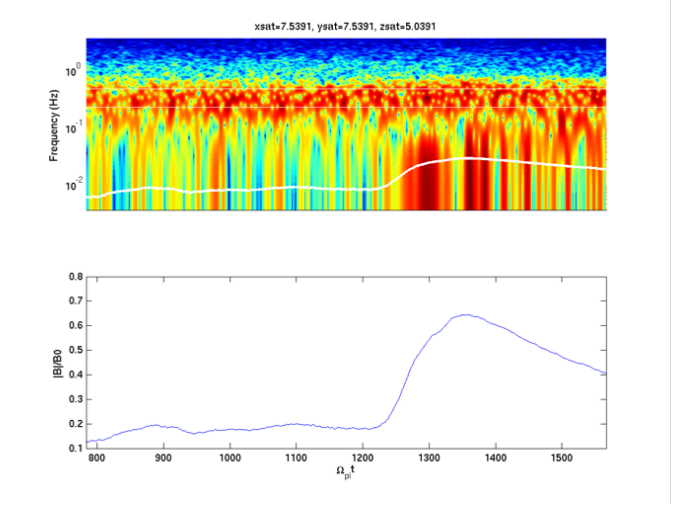

FIGURE 3. Signal from a virtual probe embedded in the simulation at $x/d_i = 7.54$, $y/d_i = 7.54$, $z/d_i = 5.04$. The top panel shows the spectrogram of the E_z signal measured. To guide the eye three frequencies are shown, from higher to lower: electron cyclotron frequency, ion plasma frequency and lower hybrid frequency. The bottom panel shows the magnetic field intensity measured by the virtual probes at the different times.

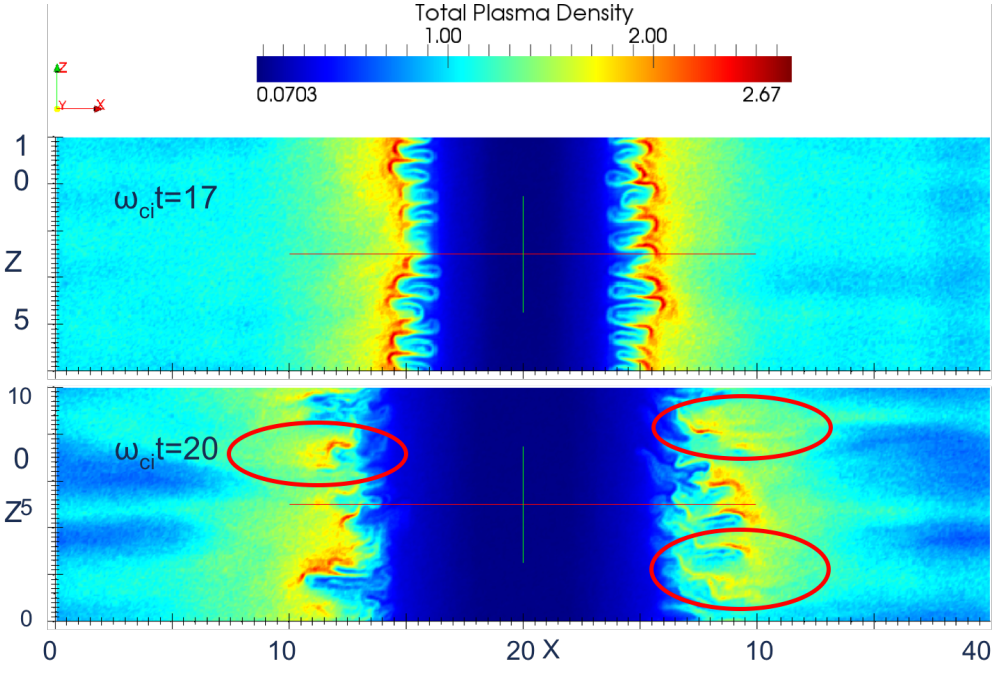

FIGURE 4. Density at the front for two different times.

where **b** is the unit vector along **B** and $E_{||}$ is the parallel component of the non ideal part of Ohm's law(Biskamp 2000), normalized as $eE_{||}/m_i c\omega_{pi}$).

A specific orientation of the magnetic field which allows for the field annihilation and energy release, is an important indicator of magnetic reconnection. In the classical two dimensional picture magnetic field lines of opposite direction approach each other and

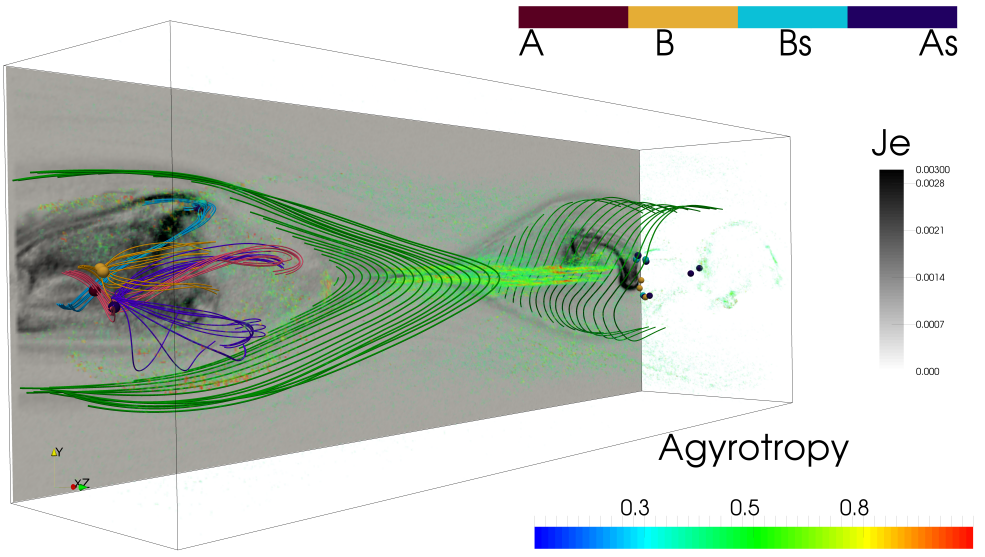

FIGURE 5. Combination of different measures a the same time: a vertical cut of the electron current intensity (grayscale); false-colour volume rendering of agyrotropy; magnetic null points (colour spheres) coloured according to their topological type. Selected field lines reconnected once at the primary site are shown in green, while secondary reconnected lines near the nulls are shown in purple, pink, orange and light blue.

form an X-point, which, extended to 3D, becomes an X-line denoted by the strong Z-aligned current in our simulation. This sort of magnetic reconnection, however, does not require the field to become exactly zero (hence, no magnetic nulls are formed) on the reconnection site. We use the technique based on the topological degree method (Greene 1992) as described in Olshevsky *et al.* (2016) to locate and classify magnetic nulls. Indeed, in the simulation reported here no magnetic nulls are present in the central current sheet as summarized in Figure 5. However, the diffusion region around the X line is characterized by strong electron agyrotropy $A = (P_{e,\perp 1} - P_{e,\perp 2})/P_{e,\perp 1} - (P_{e,\perp 2})$ that is shown with volume rendering. No strong energy dissipation is associated with the 'main' reconnection X-line.

In contrast, in the reconnection outflow a number of magnetic nulls form which are depicted by colour spheres in Figure 5. The colour denotes magnetic null's topological type: A and B (red and orange) are the three-dimensional extensions of the X-points called radial nulls; while As and Bs (light blue and blue) represent magnetic islands or magnetic flux ropes. Both radial and spiral nulls are present in the outflows, however the number of spiral ones is larger. Magnetic field lines in the vicinity of the null points in the left outflow are shown with the corresponding colours. A pair of spiral nulls is formed in a swirl of the light blue magnetic field lines, probably, driven by a shear instability. This null pair is embedded in the region of strong energy dissipation (see Fig. 5). Other nulls in this outflow are on the interfaces of magnetic fields of different polarities characterized by complex field patterns resembling an X pattern (orange) and merging into flux ropes (purple and pink). Recent observations Fu *et al.* (2017) provide a strong evidence that intermittent energy dissipation in the reconnection outflows is associated with the spiral magnetic nulls and twisted magnetic fields.

The picture provides an indication of the scenario described in the introduction: the initial reconnection site located at the centre of the box and forming a x-line produces

two outflows that become unstable and produce in turn secondary reconnection sites. In the process the plasma becomes effectively turbulent and a large fraction of the energy is converted to particle heat at these unstable fronts, rather than at the central x-line.

3. Development of intermittent turbulence in reconnection outflows

Above we have observed how reconnection tends to become visually turbulent. But is turbulence real? In a recent paper (Pucci *et al.* 2017), the properties of electric and magnetic fluctuations that are produced by magnetic reconnection have been analysed. Because of the inhomogeneous background it is important to first establish the anisotropy level and in general the 3D properties of turbulence. Analysis of the autocorrelation function of the magnetic field fluctuations have shown that the turbulence that develops in the reconnection jets is anisotropic. In particular magnetic vortexes are elongated in the direction of the background magnetic field, namely x, with a second smaller anisotropy in the yz plane. The second anisotropy becomes negligible for smaller scales and isotropy is recovered in the (k_y, k_z) plane for $k_{yz} > 1.5$, with $k_{yz} = \sqrt{k_y^2 + k_z^2}$. This allows to reduce the 3D spatial spectra to 1D isotropic spectra computed in (k_y, k_z) plane and integrated in k_x. The results of this computation shows magnetic and electric spectra with a clear power law in the sub-proton range $1.5 < k_{yz} d_p < 15$. As observed in space plasmas (Eastwood *et al.* 2009) the magnetic and electric spectra departs from each other at around $kd_p \sim 1$, the electric one proceeding with a spectral slope of ~ 1 and the magnetic one with a slope of $-8/3$. Recently Matteini *et al.* (2017), following simple dimensional arguments, have interpreted this phenomenon as due to the dominance of the Hall-effect at small scales. It is worth remarking how this interpretation still holds in such an anisotropic and inhomogeneous system, where spectra need to be carefully extracted removing large-scale background profiles and border effects.

Turbulence is responsible for the transfer of energy from fields to particles. In this work we show that this energy exchange do not take place homogeneously in the reconnection events but is located in small regions in the reconnection outflows where the energy transfer is very intense. In order to quantify the energy exchange we introduce the two dissipation proxies $D_l = \mathbf{J}\cdot\mathbf{E}$ and $D_p = \mathbf{J}\cdot(\mathbf{E}+\mathbf{v}_p\times\mathbf{B})$ (Zenitani *et al.* 2011), where $\mathbf{J}$ is the total current, $\mathbf{E}$ is the electric field, $\mathbf{v}_p$ is the proton fluid velocity, and $\mathbf{B}$ is the magnetic field. In panel (a) of Figure 7 the Probability Density Functions (PDFs) of $\delta D_l = D_l - \langle D_l\rangle_{x,y,z}$ and $\delta D_p = D_p - \langle D_p\rangle_{x,y,z}$ are plotted, where $\langle\rangle_{x,y,z}$ means average along the three axes. The two PDFs are compared with the normalized Gaussian distribution (plotted in dashed-red line). They strongly depart from Gaussian distributions, presenting instead high tails up to several standard deviations σ. In panel (b), the average D_p conditioned to a threshold current density is shown. The plot is constructed as follows: a threshold in the current density magnitude is considered and the average of D_p is computed using all those points in the domain where the value of the current is bigger than the fixed threshold. This average is then normalized to the average of D_p on all points, which gives by definition $\langle D_p|J = 0\rangle/\langle D_p\rangle = 1$. The black points in the plots represent the result of such computation for different values of the threshold. The blue curve represents the filling factors, i.e. the fraction of points used for computing the average with respect to the total number of points in the sample. The average of D_p strongly increases when higher threshold are considered up to $J/J_{rms} = 10$. Our results confirm that the exchange of energy is local, with larger values of D_p localized in very small volume filling structures. This evidence and the presence of non-Gaussian PDFs of dissipation proxies suggest that magnetic reconnection produces small scales current

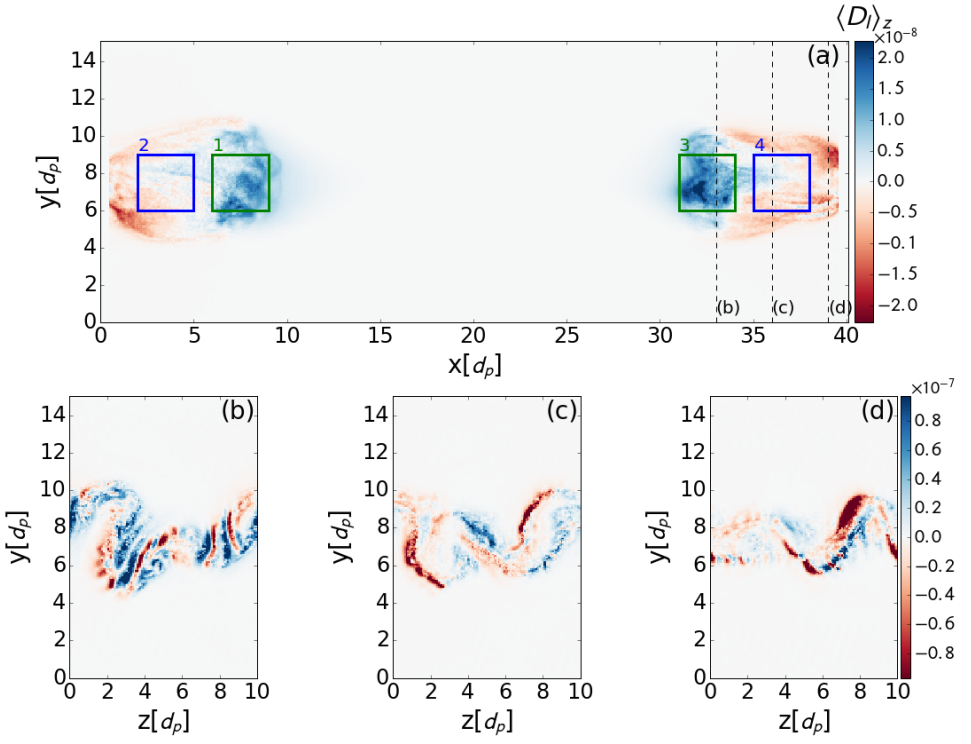

FIGURE 6. Energy exchange $D_l = \mathbf{J} \cdot \mathbf{E}$ in the xy plane averaged in the z direction (a), and in the yz plane at $x = 33\,d_p$ (b), $x = 36\,d_p$ (c), $x = 39\,d_p$ (d). The x-line is located at $x = 20\,d_p$. The three boxes in panel (a) are the ones used for the statical analysis presented in Figure 8-9.

sheets which are site of strong events of energy exchange between fields and particles. Concisely stated, all these statistics indicate that dissipation in a reconnection event is intermittent. A similar conclusion was reached by Wan *et al.* (2012) who examined the electron frame dissipation surrogate conditioned on magnitude of current density.

Figure 8-9 shows the statics of dissipation proxies presented in Figure 7 computed in sub-boxes located in the two reconnection outflows (see Figure 6). Non-Gaussian statistics and increasing conditioned average of dissipation proxies indicate that intermittent turbulence is at play in both reconnection outflows.

4. Energy Exchanges in Reconnection outflows (Gianni)

As shown in Fig. 5, the region of the outflow is characterised by intense energy exchange ($\mathbf{J} \cdot \mathbf{E}$). Recently the energy budget has been analysed in detail (Lapenta *et al.* 2016*b*) and a large fraction of the energy is deposited as particle energization, while a significant fraction is also transported by the Poynting flux.

Figure 10 reports the ion temperature at the end of the run. Ions are generally not magnetized in the reconnection region and projecting the pressure tensor in the parallel and perpendicular direction relative to the magnetic field is not productive. Ion energization in reconnection outflows and in reconnection fronts has been analysed in theory and in simulation Eastwood *et al.* (2015); Lapenta *et al.* (2016*a*). Complex processes are at play, requiring a full analysis of the phase space and of single particle trajectories to detect with accuracy the specific mechanisms accelerating the particles.

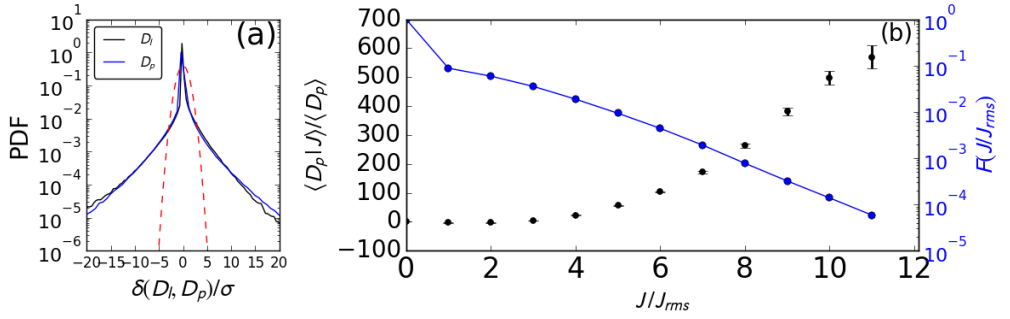

FIGURE 7. PDFs of D_l and D_p (a). Red dashed lines represent the normalized Gaussian curve. Mean D_p conditioned on local current density thresholds and (right axis) fraction F of the full box data used to compute the averages (b).

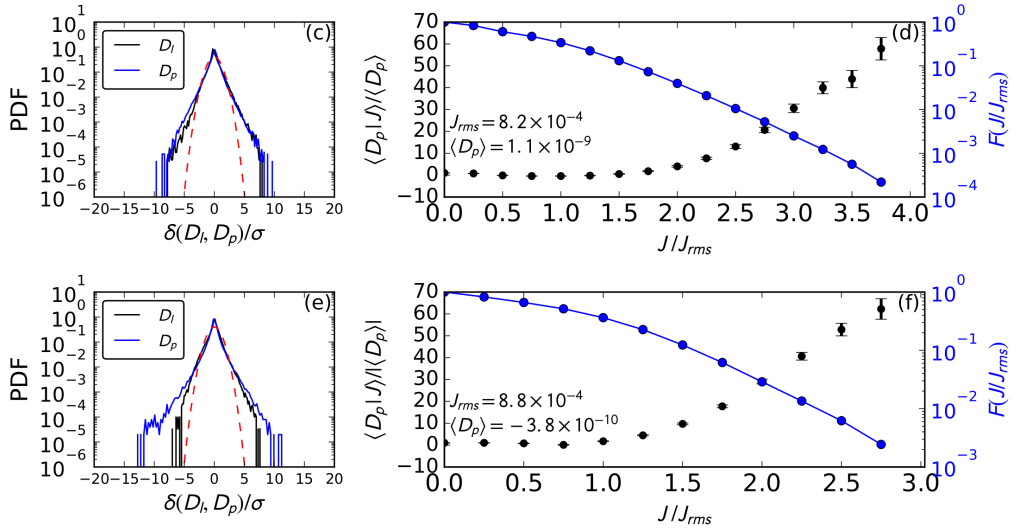

FIGURE 8. PDFs of D_l and D_p in BOX_1 (c), BOX_2 (e). Conditioned average of D_p and filling factors F in BOX_1 (d), BOX_2 (f) (left outflow).

The point of interest here is that the primary region of reconnection tends to heat the ions primarily in the y direction. This effect is due to the mixing of the two populations of ions coming from above and below from the inflow towards the reconnection region. In the outflow, instead, the plasma outflowing along the x-direction mixes with the plasma in the medium causing apparent heating in the x-direction. These effects however should not be interpreted as heating in the meaning of increasing thermodynamic temperature. The plasma is far from maxwellian and what appears as heating in the kinetic temperature (i.e. the second order moment of the distribution) is in reality the presence of multiple interpenetrating populations.

Figure **??** shows a volume rendering of the full 3D velocity probability distribution for the ions. The distribution is anisotropic and contains multiple beams. However, characterising the distribution in the form of beams is misleading because the full 3D structure displays bulges and other features that cannot be interpreted simply as beams. Multiple ion populations are present caused by different acceleration mechanisms (Eastwood *et al.* 2015).

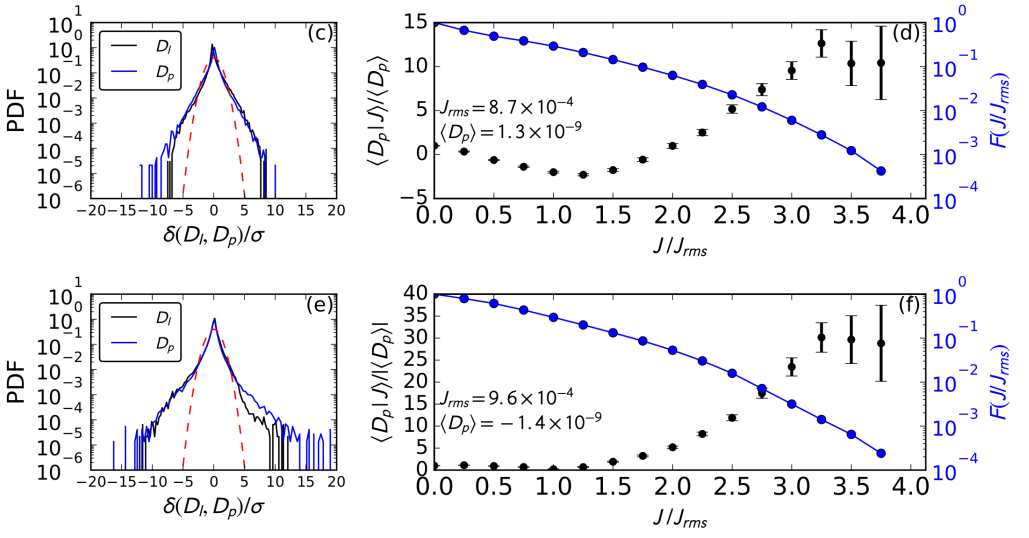

FIGURE 9. PDFs of D_l and D_p in BOX_3 (c), BOX_4 (e). Conditioned average of D_p and filling factors F in BOX_3 (d), BOX_4 (f) (right outflow).

Similarly, Fig. 12 show the parallel and perpendicular electron temperature. Again the region of instability in the reconnection outflow is characterised by strong and anisotropic electron heating.

The electron distribution is typically far smoother than the ion distribution due to the higher thermal speed. However, in the region of the secondary front instability even the electron distribution becomes complex. Figure **??** shows a volume rendering of the full 3D velocity probability distribution for the electrons computed as described above for the ions. While on a large scale the distribution is bi-maxwellian with different parallel and perpendicular temperatures, the detailed analysis shows multiple distinct populations.

REFERENCES

BISKAMP, D. 2000 *Magnetic Reconnection in Plasmas*. Cambridge University Press, UK.

DIVIN, A., KHOTYAINTSEV, Y. V., VAIVADS, A. & ANDRÉ, M. 2015*a* Lower hybrid drift instability at a dipolarization front. *Journal of Geophysical Research: Space Physics* .

DIVIN, A., KHOTYAINTSEV, Y. V., VAIVADS, A., ANDRÉ, M., MARKIDIS, S. & LAPENTA, G. 2015*b* Evolution of the lower hybrid drift instability at reconnection jet front. *Journal of Geophysical Research: Space Physics* **120** (4), 2675–2690.

EASTWOOD, J., GOLDMAN, M., HIETALA, H., NEWMAN, D., MISTRY, R. & LAPENTA, G. 2015 Ion reflection and acceleration near magnetotail dipolarization fronts associated with magnetic reconnection. *Journal of Geophysical Research: Space Physics* **120** (1), 511–525.

EASTWOOD, J., PHAN, T., BALE, S. & TJULIN, A. 2009 Observations of turbulence generated by magnetic reconnection. *Physical review letters* **102** (3), 035001.

FU, H. S., VAIVADS, A., KHOTYAINTSEV, Y. V., ANDRÉ, M., CAO, J. B., OLSHEVSKY, V., EASTWOOD, J. P. & RETINÒ, A. 2017 Intermittent energy dissipation by turbulent reconnection. *Geophysical Research Letters* **44**, 37–43.

GREENE, J. M. 1992 Locating Three-Dimensional Roots by a Bisection Method. *Journal of Computational Physics* **98**, 194–198.

HARRIS, E. G. 1962 On a plasma sheath separating regions of oppositely directed magnetic field. *Il Nuovo Cimento (1955-1965)* **23**, 115–121.

HESSE, M. & SCHINDLER, K. 1988 A theoretical foundation of general magnetic reconnection. *Journal of Geophysical Research: Space Physics (1978–2012)* **93** (A6), 5559–5567.

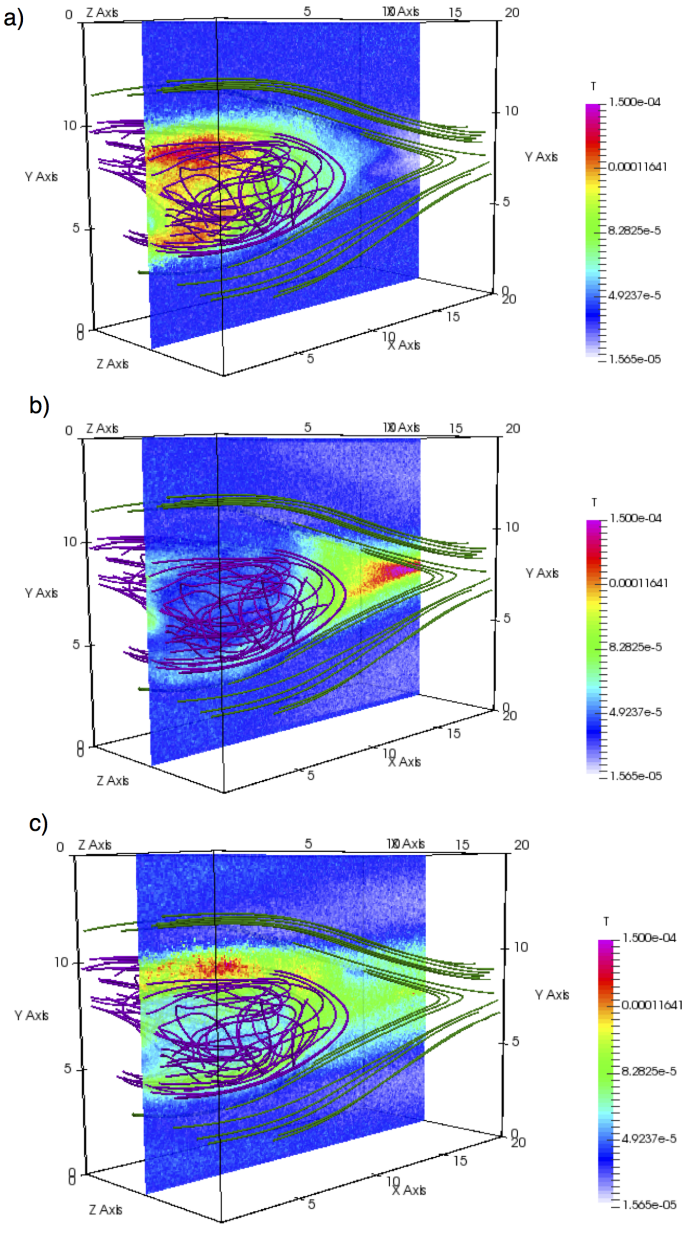

FIGURE 10. Ion temperature in the outflow: from top to bottom: T_x (a), T_y (b) and T_z (c). The left half of the domain is reported at the final time along with selected field lines.

LAPENTA, G., ASHOUR-ABDALLA, M., WALKER, R. J. & EL ALAOUI, M. 2016*a* A multiscale study of ion heating in earth's magnetotail. *Geophysical Research Letters* .

LAPENTA, G., GOLDMAN, M. V., NEWMAN, D. L. & MARKIDIS, S. 2016*b* Energy exchanges in reconnection outflows. *Plasma Physics and Controlled Fusion* **59** (1), 014019.

LAPENTA, G., MARKIDIS, S., GOLDMAN, M. V. & NEWMAN, D. L. 2015 Secondary reconnection sites in reconnection-generated flux ropes and reconnection fronts. *Nature Physics* **11** (8), 690–695.

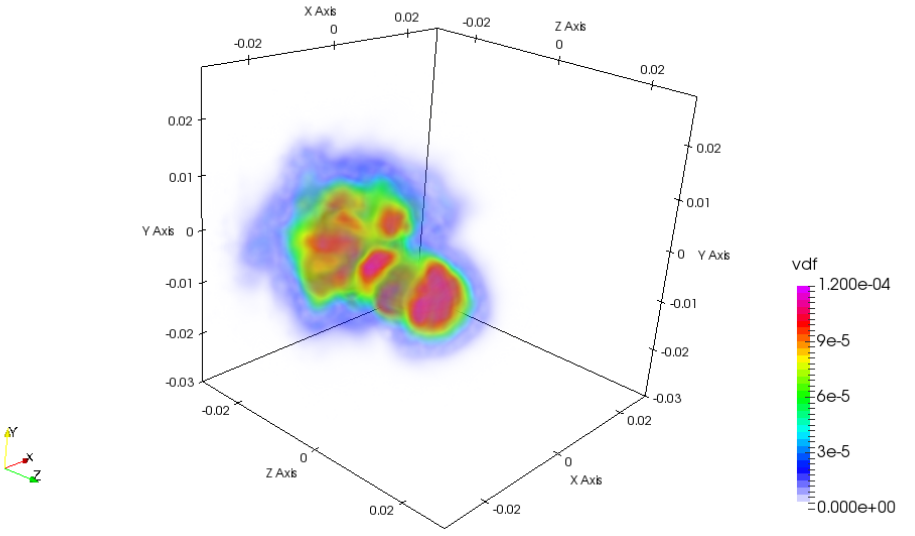

FIGURE 11. Volume rendering of the ion velocity probability distribution $f_i(v_x, v_y, v_z)$ at the position $x/d_i = 10.32$, $y/d_i = 7.5$, $z/d_i = 5$, obtained averaging over particles contained within a box centred at that location and with side $0.5d_i$.

MARKIDIS, S., LAPENTA, G. & RIZWAN-UDDIN 2010 Multi-scale simulations of plasma with iPIC3D. *Mathematics and Computers and Simulation* **80**, 1509–1519.

MATTEINI, L., ALEXANDROVA, O., CHEN, C. H. K. & LACOMBE, C. 2017 Electric and magnetic spectra from MHD to electron scales in the magnetosheath. *Monthly Notices of the Royal Astronomical Society* **466**, 945–951.

OLSHEVSKY, V., DECA, J., DIVIN, A., PENG, I. B., MARKIDIS, S., INNOCENTI, M. E., CAZZOLA, E. & LAPENTA, G. 2016 Magnetic Null Points in Kinetic Simulations of Space Plasmas. *Astrophysical Journal* **819**, 52, arXiv: 1512.02018.

PUCCI, F., SERVIDIO, S., SORRISO-VALVO, L., OLSHEVSKY, V., MATTHAEUS, W., MALARA, F., GOLDMAN, V., NEWMAN, D. & LAPENTA, G. 2017 Properties of turbulence in the reconnection exhaust: Numerical simulations compared with observations. *The Astrophysical Journal* (Accepted for publication).

VAPIREV, A., LAPENTA, G., DIVIN, A., MARKIDIS, S., HENRI, P., GOLDMAN, M. & NEWMAN, D. 2013 Formation of a transient front structure near reconnection point in 3-d pic simulations. *Journal of Geophysical Research: Space Physics* **118** (4), 1435–1449.

WAN, M., MATTHAEUS, W., KARIMABADI, H., ROYTERSHTEYN, V., SHAY, M., WU, P., DAUGHTON, W., LORING, B. & CHAPMAN, S. C. 2012 Intermittent dissipation at kinetic scales in collisionless plasma turbulence. *Physical review letters* **109** (19), 195001.

ZENITANI, S., HESSE, M., KLIMAS, A. & KUZNETSOVA, M. 2011 New measure of the dissipation region in collisionless magnetic reconnection. *Physical review letters* **106** (19), 195003.

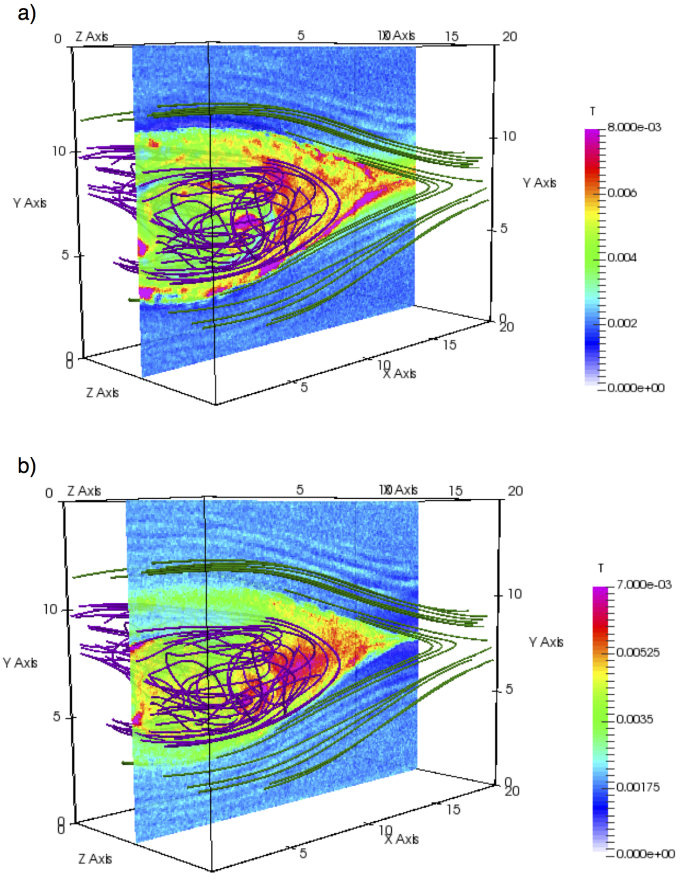

FIGURE 12. Electron parallel (a) and perpendicular (b) temperature in the outflow. The left half of the domain is reported at the final time along with selected field lines.

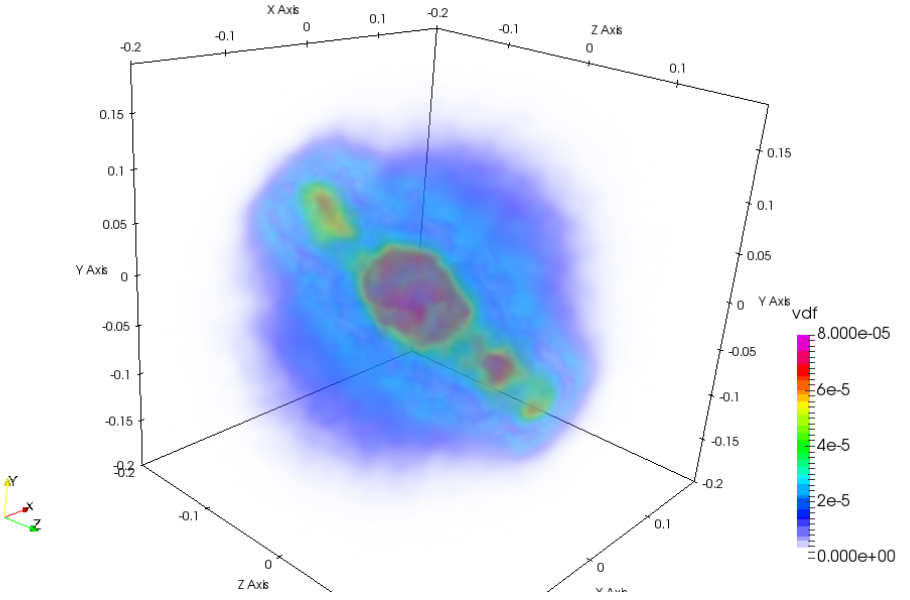

FIGURE 13. Volume rendering of the electron velocity probability distribution $f_e(v_x, v_y, v_z)$ at the position $x/d_i = 10.32$, $y/d_i = 7.5$, $z/d_i = 5$, obtained averaging over particles contained within a box centred at that location and with side $0.5d_i$.